Measurements of Tissue Optical Properties Using an Integrating Sphere Set Up

Master's Thesis
by
Emma Johansson

Lund Reports on Atomic Physics, LRAP-216
Lund, June 1997

ABSTRACT

Lasers have found many applications, such as photodynamic therapy and laser surgery, in medicine. The light distribution within the tissue is determined by the optical properties of the irradiated tissue and thus it is the optical properties of the tissue that determine the biological effect of the radiation. Many of these applications induce heat and it is therefore interesting to see how this heat affects the optical properties. In this study the optical properties of rat liver tissue were determined using an integrating-sphere set up in combination with a Monte Carlo spline interpolation program. Thermotherapy was used to induce heat in the tissue. The optical properties for the treated and untreated were compared and the result showed considerate differences in all optical interaction coefficients. Thus the effect of heat induced changes in the optical properties of tissue has to be considered for laser dosimetry applications.

Table of Contents

ABSTRACT 1

1 INTRODUCTION 3

2 THEORY 5
2.1 Light Interaction with Tissue 5
2.2 Theory for Light Propagation in Tissue 6
2.3 Monte Carlo Simulations 6

3 EXPERIMENTAL TECHNIQUES 8

4 MATERIALS AND METHODS 10
4.1 Integrating Sphere Measurements 10
4.1.1 Instrumentation 10
4.1.2 Tissue Samples 11
4.1.3 Experimental Procedure 12
4.1.4 Analysis Routine 13
4.2 Time-resolved Measurements 14
4.2.1 Instrumentation 14
4.2.2 Samples 15
4.2.3 Experimental Procedure 15
4.2.4 Analysis Routine 16

5 RESULTS 17
5.1 Integrating Sphere Measurements 17
5.2 Time-resolved Measurements 23

6 DISCUSSION 30
6.1 Integrating Sphere Measurements 30
6.2 Time-resolved Measurements 32

REFERENCES 34

1 INTRODUCTION

Determination of the optical properties of biological tissue is an important issue when it comes to certain medical applications, for example the estimation of light dosimetry requirements for laser treatment modalities. The characteristic absorption and scattering of light determine the light distribution within irradiated tissue and this information is valuable for therapeutical applications such as photodynamic therapy and laser photocoagulation. Liver tissue has been given much attention in biomedical applications. For example, laser photocoagulation in liver tissue with a Nd:YAG laser has been examined in animals.[1] Another example is tumour destruction using PDT - photodynamic therapy.[2] Also the liver is a relatively homogeneous organ which makes it possible to obtain large uniform tissue samples, which simplifies the determination of the optical properties.

Several different theoretical models, experimental techniques and approximations exist that are used to determine the optical properties of tissue. However, for a complete evaluation of the optical properties of tissue, an integrating-sphere method is usually used. The optical properties are here obtained when macroscopic measurable parameters, such as reflectance, are converted into microscopic parameters that characterize light propagation in tissue.

Light propagation in tissue is described using the general transport theory, which also is used to describe, for example, heat and mass transport. This theory gives very complex solutions and for convenience, different approximations are made to yield models that are more easy to use. Several such models exist that calculate optical properties from experimental data.[3] Kubelka-Munk theory and the diffusion theory[4] assume diffusely scattered light, while the inverse adding-doubling method[5] can be used for every set of optical properties and boundary conditions. Another model is Monte Carlo simulations that simulate the transport of individual photons through tissue.[6] These simulations are considered to yield the most exact solutions, since any geometry can be simulated by the program. A major drawback is the long computation times needed to obtain good statistics.

Many laser applications in medicine, such as laser surgery and thermotherapy, produce heat-induced changes in the optical properties of tissue. It is important to get an idea of how these changes occur and at what rate. The results can then be used to improve dosimetry and to provide information to a feedback system. This work includes investigations on how thermotherapy affects the optical properties. The goal of thermotherapy is to rapidly destroy tumours by means of heat-induced damage to the cells.

In this diploma work an integrating-sphere technique in combination with spline interpolation of previously[7] tabulated Monte-Carlo simulated values were used to retrieve the optical properties of normal and thermotherapy treated rat liver tissue.

Time-resolved measurements using picosecond laser pulses have been used for tissue transillumination. This technique is normally applied as a future alternative method for screening for breast cancer without using harmful x-rays.[8,9] The transmitted light show, at some wavelengths, large differences between normal tissue and some types of tumour tissue.[10]

In this thesis time-resolved measuremets were used to investigate the light transmitting straight through a tissue phantom composed of a polystyrene solution. The aim was to see if temporally resolving the detection could make it easier to distinguish the collimated transmittance from the diffuse transmitted light. This distinction is a source of uncertainty when measuring the total attenuation coefficient in the integrating-sphere set up.

2 THEORY

2.1 Light Interaction with Tissue

When light interacts with tissue different processes can occur; the photons can be absorbed, or scattered in the medium. Light is absorbed by various absorption centres in the tissue, so called chromophores. The cells contain different chromophores, for example vitamins and haemoglobin, which all show strongly wavelength dependent light absorption. This in turn, makes the optical absorption coefficient wavelength dependent. The *absorption coefficient*, μ_a, is the physical quantity that describes the light absorption and it is defined as the probability of a photon being absorbed in the medium per unit path length.
The dominating interaction in tissue for visible light is the elastic scattering. Elastic means that the photon energy is conserved during the scattering event. Scattering is caused by inhomogeneities in the refractive index of the medium caused by cell-membranes, cell-organells etc. The *scattering coefficient*, μ_s, gives the probability per unit path length for a photon to be scattered in the medium and thus it determines the inverse mean free path between scattering events. Furthermore, when a beam enters the tissue it will be attenuated in the forward direction according to Beer-Lambert's law. The total attenuation coefficient is defined as:

$$\mu_t = \mu_a + \mu_s \tag{2.1}$$

When a photon is scattered there is an angular scattering function associated, which states the probability of a photon to be scattered in a specific direction, characterized by the deflection angle θ. The probability distribution is often referred to as the scattering phase-function. An often used distribution is the Henyey-Greenstein phase-function,[11] initially used for interstellar dust:

$$p(\Omega' \cdot \Omega) = p(\cos\theta) = \frac{1}{4\pi} \frac{1 - g^2}{(1 + g^2 - 2g\cos\theta)^{3/2}} \tag{2.2}$$

where $p(\Omega' \cdot \Omega)$ is the probability for a photon to be scattered in the Ω-direction when the incoming direction is Ω'. The deflection angle is represented by θ. Due to the dominance of scattering over absorption in biological tissue, there are multiple scattering events before an absorption event. Thus the details of the scattering function is not important and instead an average parameter, g, is introduced. The g-factor, or anisotropy factor, is defined as:

$$g = <\cos\theta> = \int_{4\pi} \cos\theta \cdot p(\cos\theta) d\Omega \tag{2.3}$$

The value of g can vary between -1 and +1. Totally forward scattering is represented by g=1 and g=-1 represents completely backscattered light. When g=0 we have isotropic scattering. Another, often used quantity, is the reduced scattering coefficient, which describes the effective light scattering. The reduced scattering coefficient is defined as:

$$\mu_s' = (1-g)\mu_s \tag{2.4}$$

2.2 Theory for Light Propagation in Tissue

A common way of describing light propagation in tissue is to use the diffusion approximation. This method is based on the more general transport equation, which is a basic continuity equation, often used to describe heat flow. Other, than in the simplest cases, the transport equation is very difficult to solve and instead the diffusion approximation is used. To arrive at the diffusion equation the idea is to expand the functions in the transport equation into spherical harmonics, and then only use the lowest order.[12] Then the equation can be written as:

$$\frac{1}{v}\frac{\partial}{\partial t}\rho - \nabla D \nabla \rho + \mu_a \rho = \frac{1}{v} q_0 \tag{2.5}$$

where $\rho = \rho$ (**r**,t) is the photon density at position **r** at time t,

$v = c/n$ is the speed of light in the medium,

$D = \frac{1}{3\mu_{tr}} = \frac{1}{3(\mu_a + (1-g)\mu_s)}$ is the diffusion coefficient,

q_0 is a source.

The diffusion approximation is valid under the conditions that the propagating light is diffuse, which implies that the reduced scattering coefficient is much larger than the absorption, $\mu_s' >> \mu_a$. Yet, the detector have to be well-separated from the light source in order for the light to be collected as diffuse.

Another, stochastical approach of calculating the light propagation in tissue is the Monte Carlo method which is described in the following section.

2.3 Monte Carlo Simulations

A Monte Carlo simulation can be described as a random walk of photons. A photon, or rather photon packet, is traced through the medium until it exits any of the boundaries or is terminated due to absorption. This tracking procedure is repeated for

several (approximately 10^4 to 10^6) photon packets, to yield a stochastical description of the photon distribution in the medium. The advantages of the Monte Carlo method are that it can handle any geometry and the effects of boundaries are easily calculated using the laws of Fresnel and Snell.[13] The disadvantage is the many photon packets needed to obtain good statistics.

Each photon packet is initially assigned a weight, W, which is equal to 1, and then the packet is launched into the tissue. The step size, S, which is the distance to the next interaction point, is calculated as:

$$S = \frac{-\ln(1-R)}{\mu_t} \tag{2.6}$$

where R is a random number between 0 and 1.
At the new interaction point a certain amount of the photon weight is assumed to be absorbed by the medium. This amount equals ΔW:

$$\Delta W = W \frac{\mu_a}{\mu_t} \tag{2.7}$$

and thus the weight of the photon packet is reduced by this amount, yielding $W = W - \Delta W$. The next step in the simulation procedure is to calculate a new direction. The deflection angle, θ, is calculated using the Henyey-Greenstein distribution and the azimuthal scattering angle is given by $\Psi = 2\pi R$, where R is a new random number. When the weight lies below a certain limit, the photon is terminated. In this termination process, energy is lost and to compensate for this, the termination is handled by a technique called roulette. When the weight of the photon packet has reached the termination limit, the roulette gives the photon packet a probability, p, to be terminated. But there is a small chance, 1-p, that the packet survives and then the photon weight is increased by $1/(1-p)$. When all photon packets have been detected or terminated the simulation is finished.[14]

3 EXPERIMENTAL TECHNIQUES

It is the optical properties of a specific tissue that determine the distribution of light within the tissue when being irradiated. The study of light propagation in tissue is central to many biomedical applications, both diagnostic and therapeutical. Thus the determination of the optical properties of tissue is of great importance. Optical techniques and applications concerning measurements of optical properties of tissue are discussed in Ref. 3 and 15. Below a number of different techniques are described.

Time-resolved reflectance and transmittance measurements uses ultra-short (picosecond-femtosecond) light pulses. These pulses are sent through the tissue sample and the escaping light is detected at some distance from the sample. Detection is performed to give the intensity as a function of time, yielding the time-dispersion curve. Depending on the scattering and absorption properties of the medium, the time-dispersion curve is given different shapes. For a highly scattering sample the curve is broadened and if the absorption is high the intensity of the time-dispersion curve is decreased. The optical properties in terms of μ_s' and μ_a can then be determined by comparing this curve with a light propagation model,[16] such as the diffusion approximation, if valid. As previously mentioned, this is true when the scattering is much larger than the absorption, and if the observation point is located far enough away from the point of entry of the light.[17] A streak camera system is often used as a detector in time-resolved transillumination measurements.[8,18] The technical principle of the streak camera is much like that of an oscilloscope. There is an adjustable slit at the entrance of the camera. This slit is focused onto a photo cathode inside the streak camera and when photons hit the cathode, electrons are emitted. The electrons are accelerated towards a phosphorus screen by a high voltage. When they hit the screen light is emitted, amplified by an image intensifier. A high voltage, applied transversely to the path of the electrons, can deflect them. By ramping this high voltage it is possible to obtain an image where different positions on the screen correspond to the different arrival times of the electrons. This gives an image that has time on the x-axis and the image of the slit on the y-axis. The time-resolved diffusion approximation technique has for example been used for breast tissue transillumination[19] where the aim is to detect cancer tumours. This is possible as the optical properties of malignant tissue differ from those of normal tissue. Temporally resolving the detection also makes it possible to get a higher spatial resolution by excluding the multiscattered photons. Here only the first arriving photons, the ones travelled the shortest pathlength, are detected.[20-22] This technique is often referred to as time-gating. Furthermore, if the light source consists of white light it is possible to determine the optical properties at all wavelengths simultaneously.[23,24] The time-resolved transmittance technique can also be used for studying paper and plant material.[25]

In the *frequency-domain* reflectance and transmittance technique, intensity-modulated light is sent through the tissue.[26-28] The phase shift and the demodulated light is then detected at a certain distance from the light source. Measurements of the phase shift, ϕ, and the amplitude modulation, M, at a frequency where $0<M<1$, give both μ_a and μ_s'. The advantage compared to the time-domain is that the frequency can be varied so that boundary effects due to the finite extension of the tissue, show less influence on the result. Also the aquisition time is short enough to enable monitoring of dynamic phenomena such as changes in hemoglobin oxygenation.

Sending CW light into tissue gives a *spatial distribution of the fluence* that is determined by the optical properties of the tissue.[29,30] The light intensity is detected as a function of the distance from the entering point.[31] This radial distribution of the fluence is then fitted to a model, for example the diffusion approximation and the optical properties can be extracted.

Continous light is also used by the *integrating-sphere technique*. A sphere with its inner surface covered with a highly reflecting barium sulfate coating is here collecting the detection light. This technique uses thin tissue slices *in vitro* as samples.[32] A collimated light beam is impinging on a thin tissue sample and the total transmittance, T_{tot}, and the diffuse reflectance, R_{diff}, is measured using the integrating sphere. The transmitted unscattered part, T_{coll}, is collected in a narrow-beam setup, where the light is detected far away from the sample and the diffuse transmitted light is suppressed by various filtering.[33] From these three parameters it is possible to obtain the optical coefficients of the tissue, μ_a, μ_s and g. To associate the optical properties to the three measured quantities, a photon propagation model like Monte Carlo simulations is preferable. The reflectance and transmittance can be calculated for a large set of optical properties and this data base can then be used as a look-up table. Together with an interpolation technique the optical properties can be determined.[7]

This work applies two of the described techniques: the integrating-sphere method and time-resolved transmittance measurements.

4 MATERIAL AND METHODS

4.1 Integrating Sphere Measurements

The purpose of these experiments was to investigate the influence of thermotherapy on the optical properties of rat liver tissue. Optical properties for both treated and untreated tissue was determined and compared.

4.1.1 Instrumentation

Figure 4.1 shows the experimental setup that was used in the integrating sphere and the collimated beam measurements.

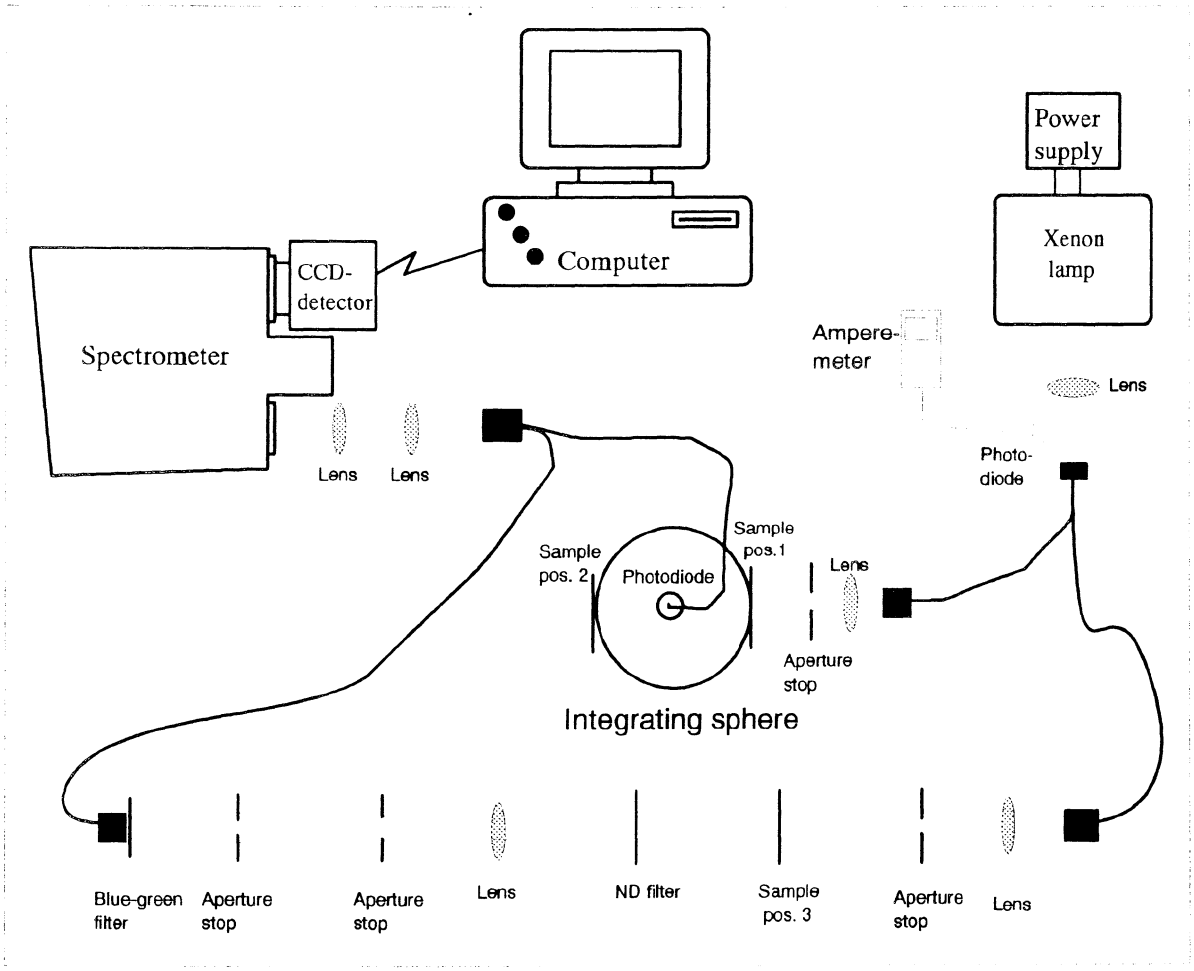

Fig 4.1 Setup for the integrating sphere and the narrow-beam measurements. By placing the sample in position 1,2 and 3 respectively the total transmittance, the diffuse reflectance and the collimated transmittance were measured.

The light source was a 75-W high-pressure Xenon lamp which was cooled with water. To control the output power a photodiode was placed just by the lamp. The light from the lamp was focused into two optical fibres, both with a core diameter of 600 μm, by a 12-cm-focal-length lens. The distal end of one of the fibres was connected to the sphere (Oriel), which was 20.3 cm in diameter and had an inner surface covered with barium sulfate. The light beam was collimated by a 8-cm-focal-length lens and an aperture stop resulting in a beam diameter of 4 mm at both sample positions of the sphere. The totally transmitted and the diffusely reflected light was measured by placing the sample at the entrance and exit port, respectively. When the measurement of the total transmittance was performed a reference plug, with the same coating as the rest of the sphere, was placed in the exit port. A baffle on the inside of the sphere blocked the specular reflected light from the sample at the exit port from being detected. The light flux filling the sphere was probed by a 5 mm-diameter fibre bundle with its distal end focused on a spectrometer (Spex 270M). To measure the collimated transmittance a narrow-beam experiment was conducted. The transmitted light was detected far away from the sample position. Aperture stops prevented the diffuse transmittance from being detected. A bluegreen filter was used to suppress the light in that wavelength region, so that second order peaks would not be detected. The collimated light beam was coupled into a 5 mm-diameter fibre bundle and focused on to the spectrometer slit. A handscan unit was used to remotely control the spectrometer. The slit width of the spectrometer was set to 75 μm and a 150-grooves/mm grating was used. To be able to cover the wavelength region of interest: 600-1050 nm, the centre wavelength was adjusted to 845 nm.

Light detection was made by a CCD-detector with a chip size of 330 x 1100 pixels. The detector was cooled to -40°C to minimize the dark current. The CCD-detector and the spectrometer were controlled by a personal computer.

4.1.2 Tissue Samples

Thermotherapy

In thermotherapy the tissue is heated to temperatures above 50°C. This leads to thermal coagulation which destroys the cells in the treated area. With this method it is possible to treat port wine stains and a condition called benign prostatic hyperplasia. The heat can be induced in different ways. For example by microwaves, which are used both non-invasively and invasively, by ultrasound and by laser light.[34] Here laser light from an Nd:YAG laser was used to raise the temperature.

Sample Preparation

For the integrating-sphere measurements, tissue samples from rat liver were used. In all twelve rats were used, giving 19 liver samples. The animals were first anaesthetized before the abdomen was cut. Thermotherapy was induced in the left liver lobe using a continuous wave Nd:YAG laser (Mod. 416, Quantronix Corp.,

Smithtown, NY, USA), emitting radiation at 1064 nm. A 40 times magnification microscope objective lens focused the light onto a 1 cm diameter spot on the liver surface, which gave a radiation intensity of 2.5 W/cm^2. The temperature was measured in the centre of the irradiated spot, approximately 3 mm below the tissue surface, every other second during the treatment. Laser-induced thermotherapy was performed for 20 minutes inducing an increase in the tissue temperature to 57.7 ± 5.9°C (mean ± one standard deviation). The treatment introduced a change in colour in the illuminated tissue area, from dark red to almost black., with a surrounding region that was slightly less coloured. Directly after the treatment the left liver lobe was excised. After a time delay that matched the time needed for the optical measurements, the untreated right lobe was also excised. The animals were then sacrificed by an overdose of anaesthetic drug. A thin slice (approximately 1.5 mm in thickness), was cut from the liver tissue, including the irradiated spot for the treated samples. The slice was placed between two glass slides, 1.0 mm thick, and separated by two 1.0 mm thick spacers. Two clamps were used to compress the liver sample to 1.0 mm thickness. The sample size was approximately 3x3 cm. This procedure was repeated for ten animals, resulting in nine treated samples and ten untreated samples.

4.1.3 Experimental Procedure

Calibration

Wavelength calibration of the CCD-camera connected to the spectrometer was performed using the known atomic emission lines from a mercury discharge lamp and from the Xenon lamp. The light from the lamps was imaged onto the entrance slit of the spectrometer and a calibration spectrum was accumulated. By the use of more than three emission lines and the fact that the wavelength of the centre pixel was approximately 845 nm, a calibration was made. Next a calibration of the integrating sphere was performed. To do this, a set of four NIST-traceable calibration plugs (Oriel, approximative reflectance of 2%, 50%, 75% and 99%) with tabulated reflectance in the wavelength region 250 - 2500 nm were used. A spectrum was collected for each plug, and the intensities of the 2, 50, 75 and 99% calibration plugs were divided by the intensity of the reference plug with an approximate reflectance of 99%. These ratios were compared with the corresponding theoretical ratios. Finally a calibration of the integrating-sphere and the narrow-beam setup was made. A suspension of polystyrene spheres with a diameter of 2 μm was diluted in distilled water to concentrations yielding scattering coefficients in the range of those of liver tissue. The scattering coefficients were derived from Mie-scattering calculations.[35, 36] Measurements were made with the polystyrene suspension in a glass cuvette with a thickness of 1.0 mm.

Measurements

First a background spectrum was accumulated with both light beams blocked. All other measurements could then be made without the influence of the background

light, by automatically subtracting the background spectrum. For the sphere measurements an aquisition time of 15x3 seconds was used and for the collimated beam setup the aquisition time was slightly longer, 15x5 seconds. The reference intensity, I_{ref}, was measured for the sphere with the highly reflecting barium sulfate reference plug in the exit port. By placing the sample in sample position 1 and keeping the barium sulfate plug in the exit port, I_T , the total transmitted light flux, could be measured. The sample was then moved to sample position 2, the exit port, giving the intensity of the diffusely reflected light, I_R. From I_{ref}, I_T and I_R the transmittance and reflectance were obtained by

$$T = I_T / I_{ref} \tag{4.1}$$

$$R = R_{BS}(I_R / I_{ref}), \tag{4.2}$$

where R_{BS} is the tabulated reflectance factor for the barium sulfate reference plug. Next the sample was placed in position 3 and the intensity of the unscattered transmission, I_{coll}, was measured. For the reference measurement in the collimated beam setup, a water cuvette was placed in the sample position 3, and the reference intensity, I_o, was recorded. Schott neutral density (ND) filters were used to yield measured reference and sample intensities in the same range in order to avoid unlinear effects due to the detector. The attenuation coefficient could then be determined as

$$\mu_t = -\ln[(I_{coll} / I_0)(T_{ND})] / d, \tag{4.3}$$

where T_{ND} is the transmittance of the neutral density filters used for the I_o measurement and d is the thickness of the sample, here 1 mm.
For each sample position, measurements were made at three different positions on the tissue surface, resulting in 3 x 3 x 19 = 171 raw spectra recorded in total for the setup.

4.1.4 Analysis Routine

All spectra were corrected for perturbation peaks, caused by the detection of cosmic radiation. To make the further evaluations of the spectrum more effective, a mean value was calculated over six datapoints, decreasing the number of points in each spectra to 184. A data set composed of R, T and μ_t- spectra was then used as input parameter to a Monte Carlo spline interpolation program, performed on a Pentium 133 MHz computer. The program interpolated among previously Monte Carlo calculated reflectance and transmittance values obtained from different sets of optical properties[7] and fitted the measured data to those calculated and returned the corresponding optical interaction coefficients. Thus, output parameters were μ_a, μ_s and g.

4.2 Time-Resolved Measurements

Time-resolved measurements were made to investigate the influence of the scattered light on the collimated transmittance of a polystyrene solution as well as of human blood.

4.2.1 Instrumentation

A schematic drawing over the experimental setup is shown in Fig. 4.2.

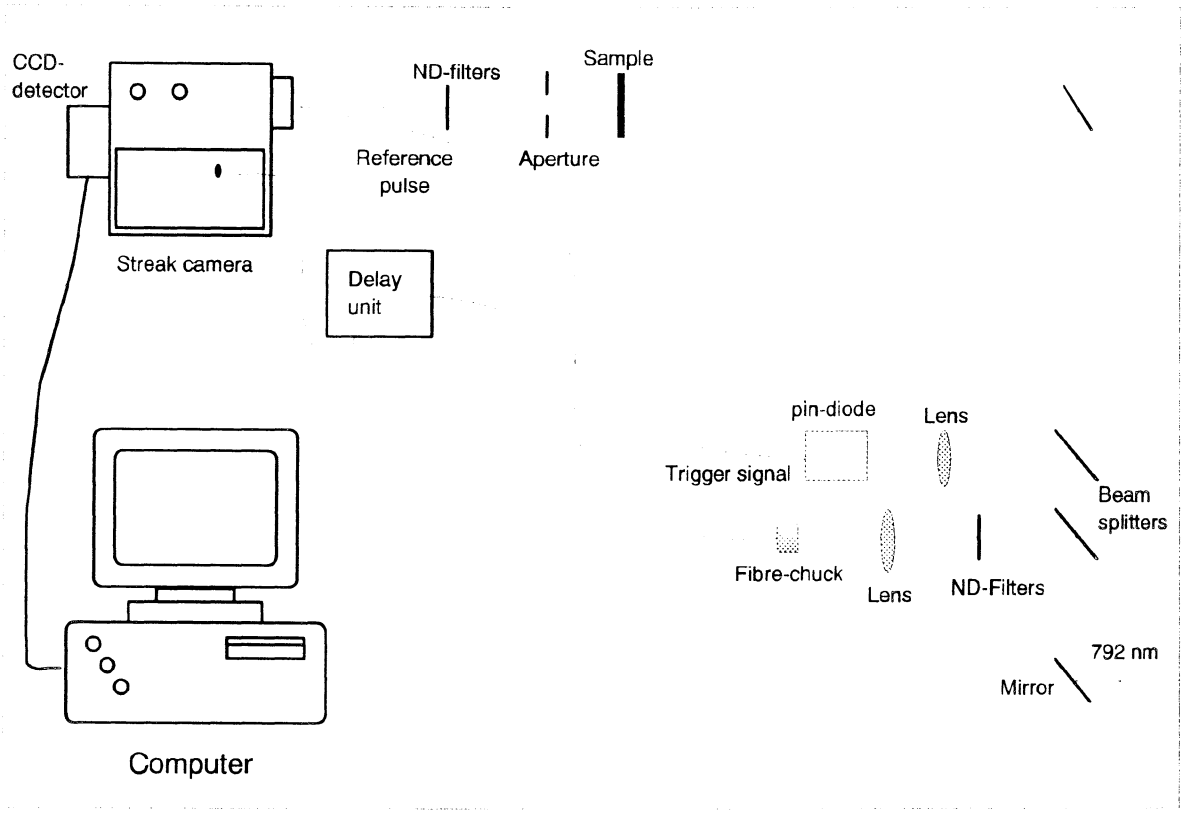

Fig. 4.2 The experimental set up for the time resolved measurements. The Ti:sapphire laser light was guided, through a tube, from the room across the hall.

An argon-ion-laser-pumped passively modelocked Ti:sapphire laser was used as a light source.[37] Approximately 100-fs-long pulses with a wavelength of 792 nm were produced with a repetition rate of 76 MHz. The incoming light was deflected by a mirror and a beam splitter was used to send a small part of the beam through an optical fiber, whose other end was directed to illuminate the slit of the streak camera This signal was used as a reference signal and gave the apparatus function. Another part of the beam was focused onto a photodiode (Hamamatsu pindiode head C1808), which gave a trigger signal to the syncroscan streak unit (Hamamatsu M1955). This

enabled the scanning frequency of the streak camera to be syncronized with the repetition frequency of the train of laser pulses. A delay box was used to separate the reference and sample signals in time, so that both could be viewed at the same time on the computer screen. The sample was placed between two aperture stops to prevent the scattered light from being detected. A couple of Schott neutral density (ND) filters were used to decrease the light intensity in order to protect the detection system from overflow. ND filters were also used to attenuate the reference pulse, so that its amplitude was comparable with the amplitude of the sample pulse. A streak camera[8,38] (Hamamatsu C1587) and a two-dimensional CCD camera (Hamamatsu C3140) were used for light detection. The slit of the streak camera was opened to approximately 20 μm for all samples. The CCD camera was controlled by a computer and thermoelectrically cooled to -30°C. At the position of the sample the beam diameter was 4 mm and the aperture stop opening was held at 2.5 cm except for one set of measurements where it was 1.5 cm. The distance between the sample and the aperture stop, and the sample and the slit was 10 cm and 52 cm respectively.

4.2.2 Samples

For the time-resolved experiments two different polystyrene solutions were used, one containing 1 μm-spheres and the other containing 2 μm-spheres, diluted in water to seven different concentrations of polystyrene spheres, 20, 30 ,40 ,50, 60, 70, 80, 90 and 100%. The solution was contained in a cuvette made of two glass slides each with a thickness of 1.0 mm, separated by two or four 1.0 mm spacers, respectively, giving one cuvette with a sample thickness of 1.0 mm and one of 2.0 mm. The sample area was approximately 4.0 x 2.5 cm. In one of the measurements an absorber (ink) was added to the sample solution. A 1% ink solution was prepared, and different concentrations, 20, 40, 60, 80 and 100%, of this solution was used to dilute the 100%-polystyrene solution. For all these measurements the total polystyrene concentration was 70%. Also a few measurements were made with human blood diluted with saline to 25, 50 and 100%.

4.2.3 Experimental Procedure

First the background intensity measurements were made with the streak camera shutter closed. An aquisition time of 10 x 5 s were used for all the measurements. The sample was then placed in the sample holder and the slit of the streak camera was opened to approximately 20 μm. Then an aquisition was made and the image recorded by the CCD-camera was stored as a raw data image. In addition, a profile, the so called time dispersion curve, was formed by the timescale, and the corresponding intensity, of the image. For every sample, five measurements were made and the average value was calculated. This procedure was repeated for all samples. The aperture stop which was placed 10 cm behind the sample, was used to investigate its effect on the amount of detected light. A comparison was made between an opening

of 1.5 cm-diameter and one of 2.5 cm-diameter. For one series of measurements an integrating sphere was placed in the light beam and the sample was placed in the entrance port of the sphere. This is how the narrow-beam measurements are most often performed. Also measurements were made with a lens placed after the sample, between it and the aperture stop, to see if this made any difference to the amount of collected light. Some blood was donated by the author and measurements were made with a sample thickness of 1.0 mm for three different concentrations, 25, 50 and 100%.

4.2.4 Analysis Routine

Measurements were made for two different sample thicknesses, 1.0 and 2.0 mm, and two different diameters of the aperture stop, 1.5 and 2.5 cm, placed 10 cm behind the sample. The FWHM - full width half maximum - value from the time dispersion curves, was plotted versus the scattering coefficient, which was known for the undiluted polystyrene solution (see section 3.1.3) and easily calculated for the other concentrations. For the blood measurements a tabulated value[3] of the scattering coefficient was used.

5 RESULTS

5.1 Integrating Sphere Measurements

Calibration

Fig 5.1 shows the result from one of the measurements of the calibration plugs. The deviation in percent of the measured ratio(calibration plug intensity divided by reference plug intensity), from the theoreticalratio. The curve in figure 5.1 corresponds to data from the calibration plug having an approximate reflectance of 50%, a value rather close to the reflectance values of liver tissue, approximately 30%. An error of 2-5% was obtained.

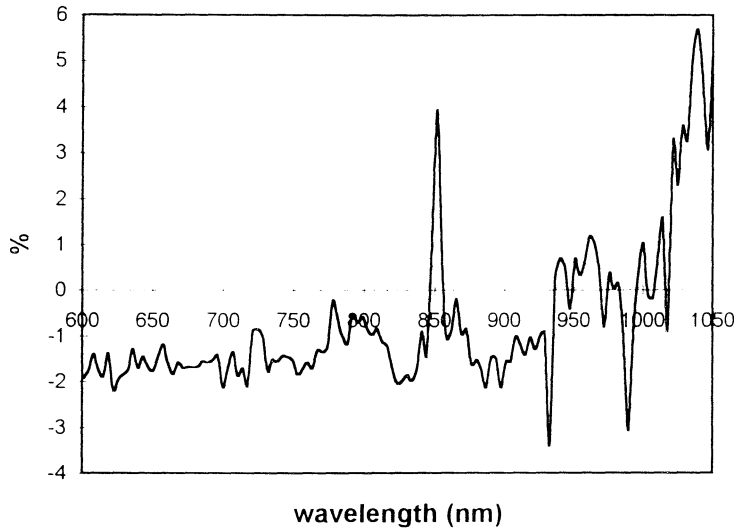

Fig 5.1 *The deviation in percent of the measured reflectance from the theoretical for the 50% calibration plug.*

The calibration measurements performed with the polystyrene solutions showed good agreement with the Mie-scattering calculations. The mean deviation for the 5% solution was 9% and for the 7.5%-solution it was 10%. In figure 5.2 a comparison is shown between the measured values and the calculated values of the scattering coefficient μ_s for two different concentration of polystyrene spheres- 5% and 7.5%. These concentrations were chosen as they yield optical properties in the range of those for liver tissue.

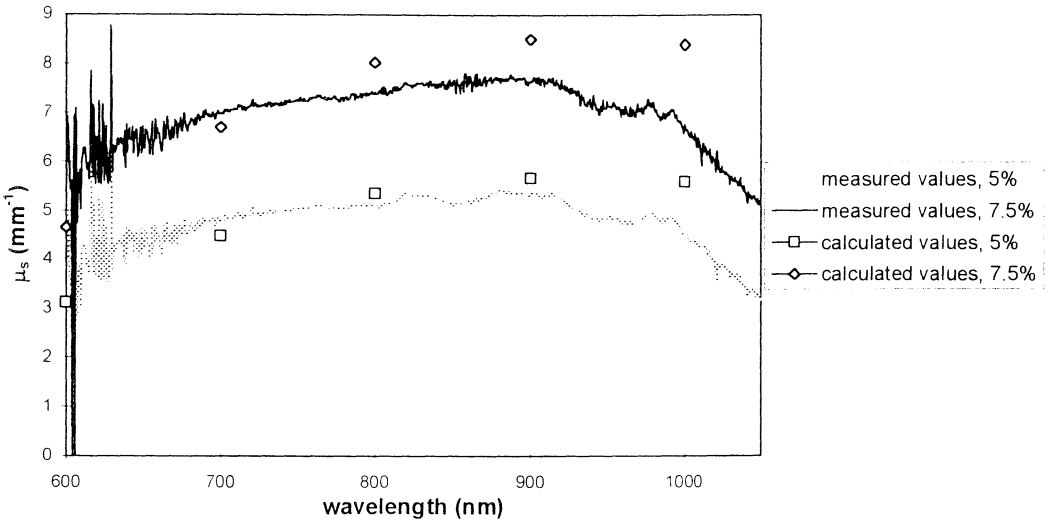

Fig. 5.2 Comparison of measured and calculated values of μ_s for two different polystyrene concentrations. 5% and 7.5% The scattering coefficient is plotted versus the wavelength..

Optical Interaction Coefficients before and after Thermotherapy

Figures 5.3 a-d presents the mean values of the optical interaction coefficients, measured before and after thermotherapy. A separation was made between the centre of the treated region and the periphery of the same, as there was a clear difference in the visible colour of these two. At 800 nm the mean value of the absorption coefficient, μ_a, for all ten untreated samples was 0.10 mm^{-1} with a standard deviation of 0.02; the scattering coefficient μ_s was 8.3 ± 0.2 mm^{-1}, the g factor 0.87 ± 0.02. The reduced scattering coeffcient μ_s', was thus 1.1 ± 0.2 mm^{-1}. For the treated tissue in the centre, the corresponding values were on average: μ_a = 0.31 ± 0.10 mm^{-1}, μ_s = 10.2 ± 0.7 mm^{-1}, g factor = 0.67 ± 0.07 and μ_s' = 3.4 ± 0.9 mm^{-1}. In the peripheral region of the treated tissue the results were: μ_a = 0.25 ± 0.08 mm^{-1}, μ_s = 9.7 ± 0.6 mm^{-1}, g factor = 0.70 ± 0.07 and μ_s' = 3.0 ± 0.8 mm^{-1}. In figures 5.3 a-d. the mean values of the optical properties for the different regions are shown together with the standard deviation at approximately 820 nm for the untreated and treated central tissue areas.

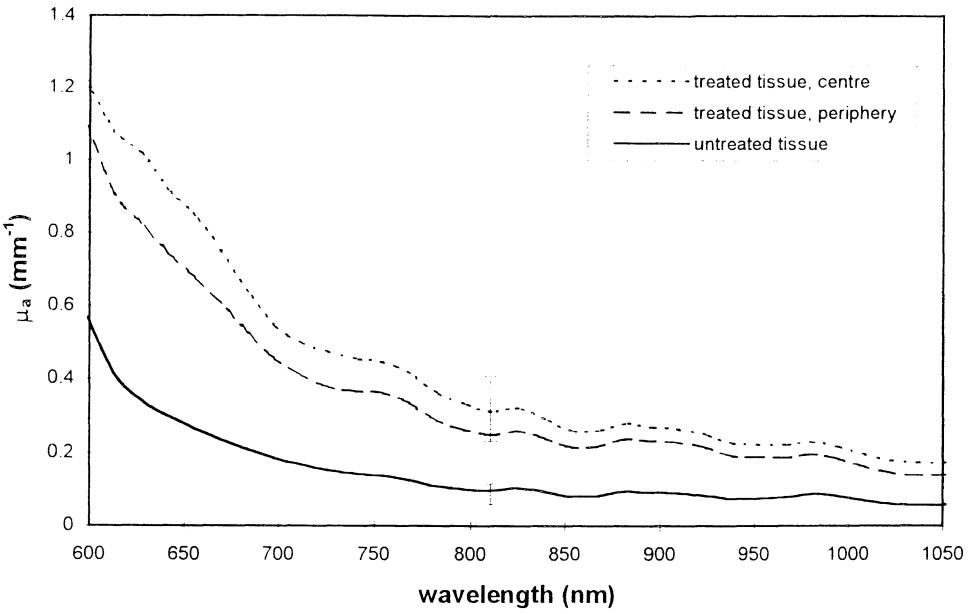

Fig. 5.3 a The graph shows the mean values of the absorption coefficient, for the different regions. The standard deviation at approximately 820 nm is shown.

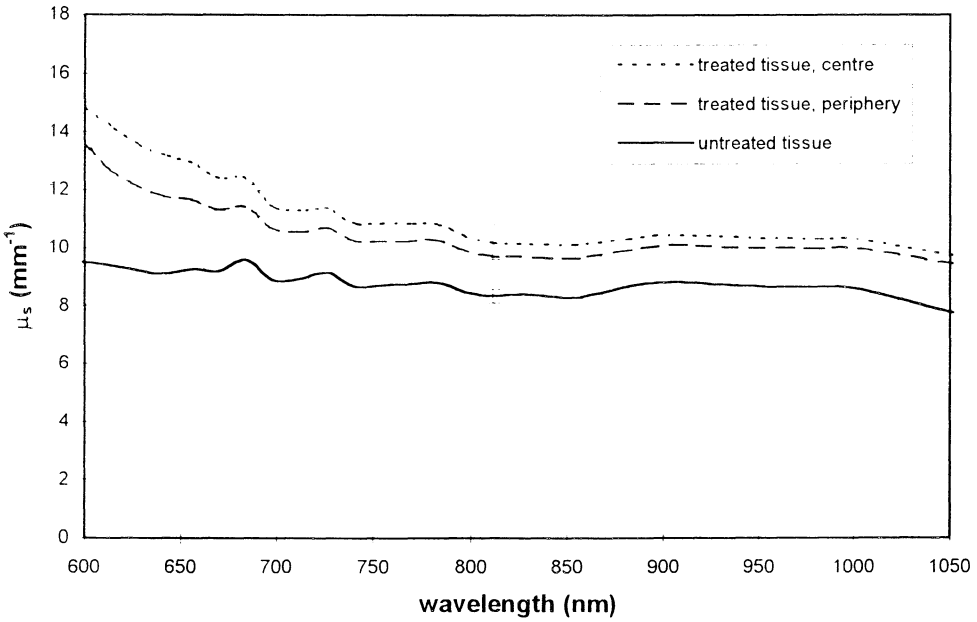

Fig. 5.3 b The mean values of the scattering coefficient versus the wavelength.

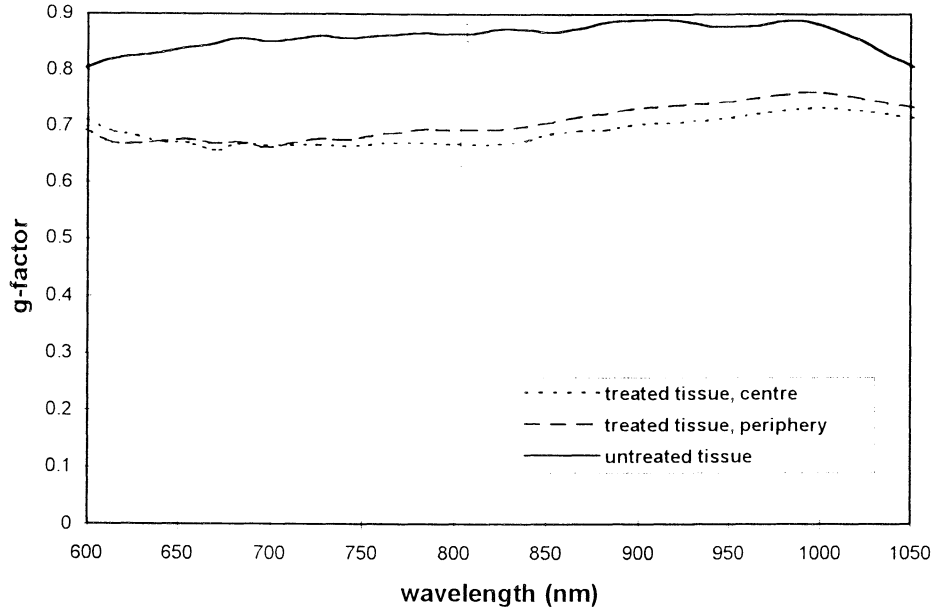

Fig. 5.3 c The mean values of the g- factor plotted against the wavelength.

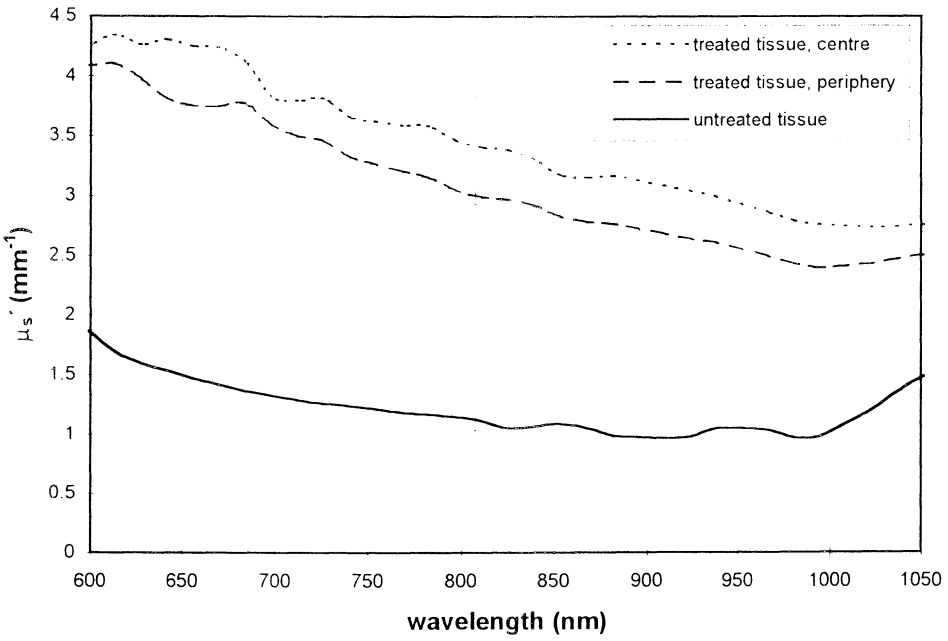

Fig. 5.3 d The mean values of the reduced scattering coefficient versus the wavelength.

The change in the optical properties due to thermotherapy was also calculated. The relative change in the anisotropy factor (in percent) was calculated by:

$\Delta g = 100[g(\text{treated}) - g(\text{non-treated})]/g(\text{non-treated})$.

Similar calculations were performed for the absorption, scattering and reduced scattering coefficients. The relative changes in all the respective optical properties were averaged to give an overall view of the effects of the thermotherapy treatment. The results are shown in figures 5.4 a-d together with the standard deviations at approximately 800 nm for the central region of the treated tissue. All optical interaction coefficients show a clear relative change between treated and untreated tissue. A manifest change of 200 % is seen in the absorption coefficient. For μ_s the average increase is 20-25 % and the g-factor is decreased by on average 20 %. The reduced scattering show an increase of approximately 200 %. These values are related to central areas, for the peripheral region the effect is somewhat smaller, also shown in figures 5.4 a-d.

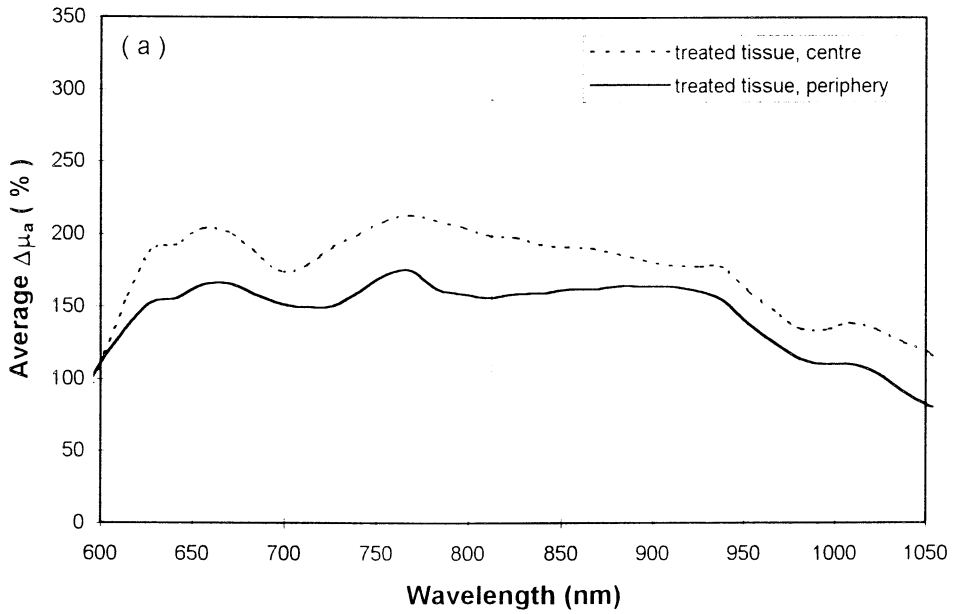

Fig. 5.4 a Average change in the absorption coefficient after thermotherapy. The bar represents the standard deviation for the central region.

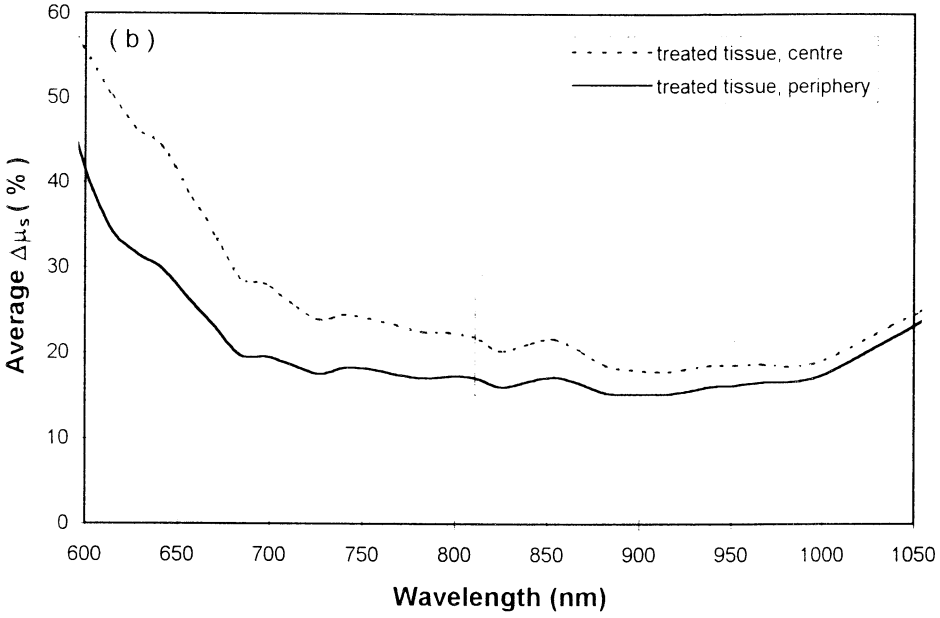

Fig. 5.4 b Average change in the scattering coefficient after thermotherapy. The bar represents the standard deviation for the central region.

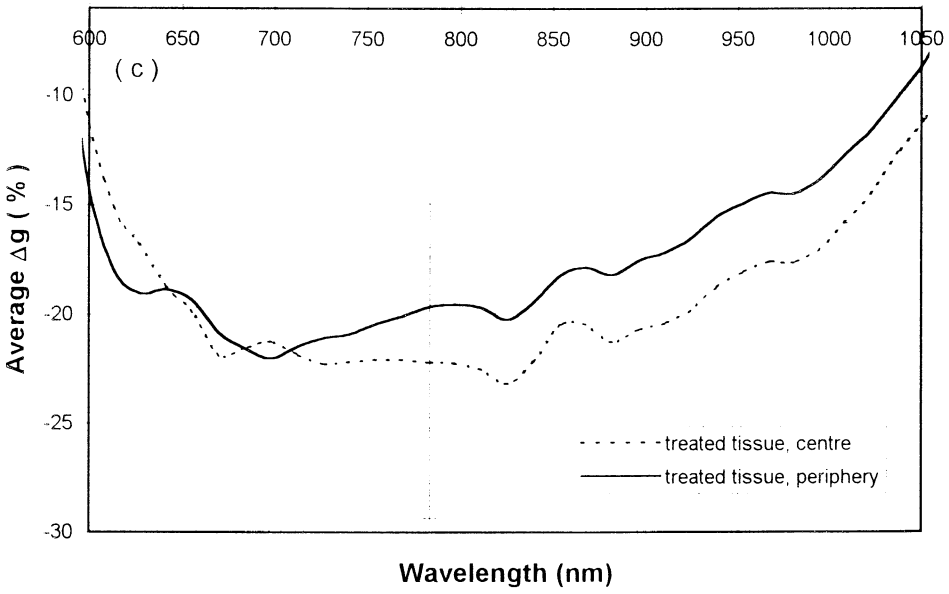

Fig. 5.4 c Average relative change for the g-factor for treated tissue in the centre and periphery. The standard deviation for the central region is shown.

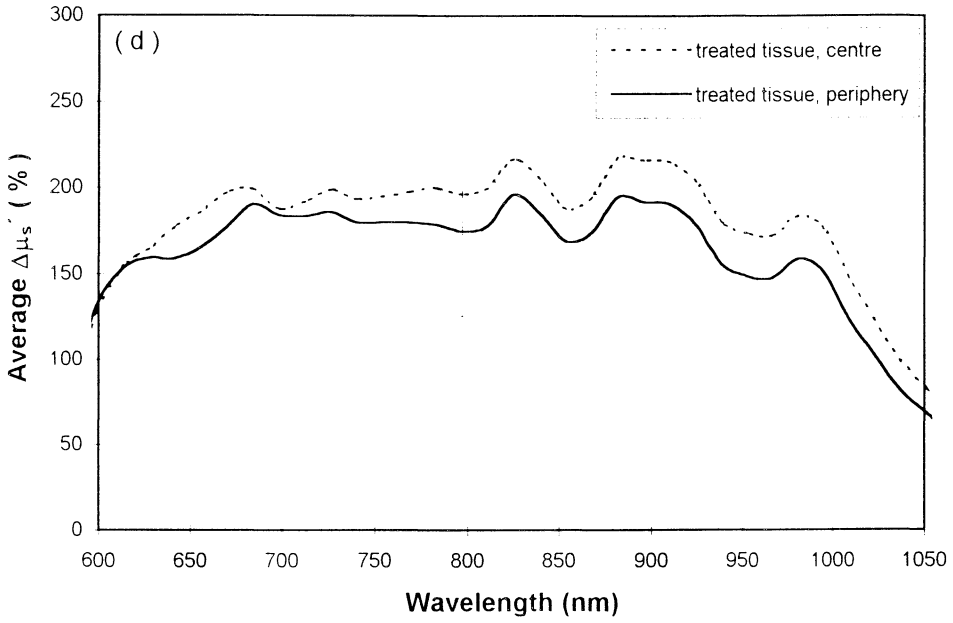

Fig. 5.4 d Average relative change for the reduced scattering coefficient for treated tissue in the centre and periphery. The standard deviation for the central region is shown.

5.2 Timeresolved Measurements

The time-resolved measurements were made in order to examine how accurate the collimated beam measurements in the integrating sphere set up were. With the time dispersion curve it is easier to distinguish the collimated photons from those that have interacted with the tissue. In figure 5.5 the typical time dispersion curves for the reference pulse and the sample pulse, respectively, are shown.

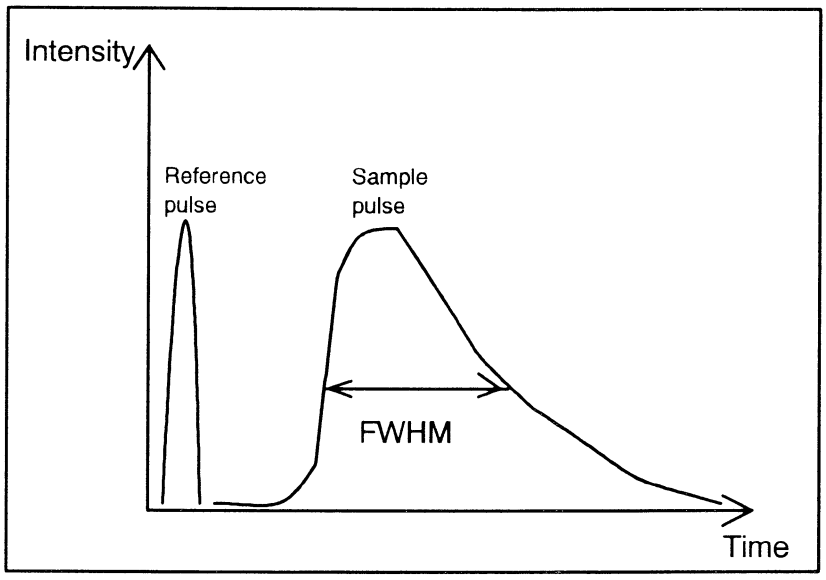

Fig. 5.5 *The time dispersion curves for the reference pulse and the sample pulse are shown. The FWHM-value is indicated in the sample curve.*

Experiments were made with polystyrene-concentrations in the range of 20-100%. This corresponds to a scattering coefficient of 20-106 mm^{-1}.[36] The polystyrene-spheres are non-absorbing, $\mu_a=0$. In figure 5.6 we can see that the FWHM increases with increased scattering coefficient. The FWHM of the reference pulse varied somewhat but was approximately 14 ps. Furthermore, measurements with two different sizes, 1.5 and 2.5 cm, of the aperture were performed, and as can be seen in figure 5.6 the FWHM does not increase with increasing aperture in this range. If the two curves are adjusted so that we get a linear relation between the FWHM and the scattering coefficient, these lines can be extrapolated to the scattering coefficient of liver tissue, approximately 10 mm^{-1}. At this scattering coefficient value, the difference in the FWHM is 1.5 ps.

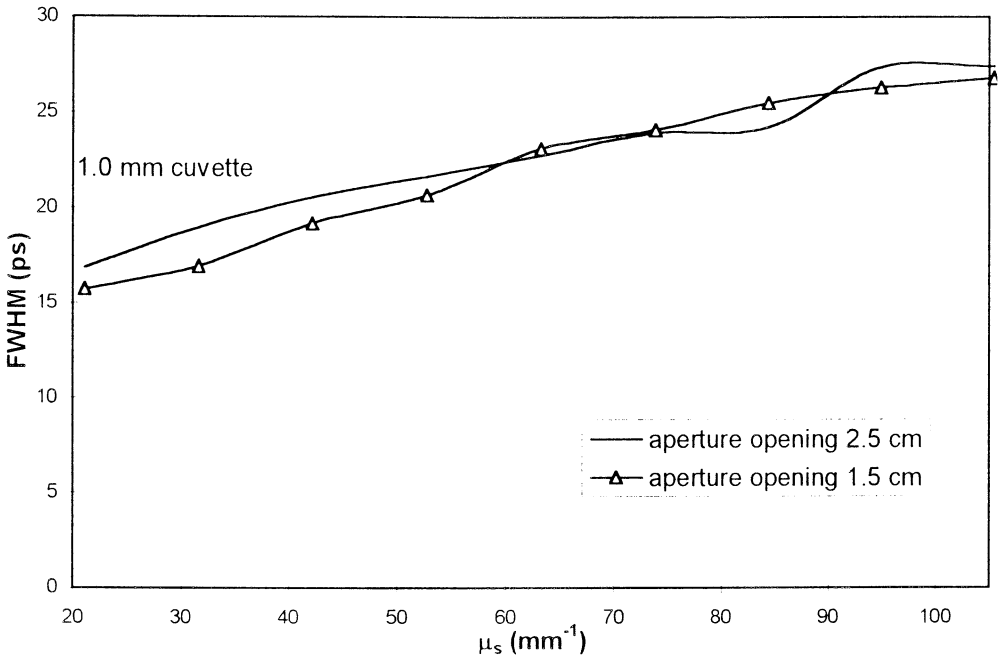

Fig 5.6 The influence of the scattering coefficient on the FWHM. Also the effect of different aperture openings on the FWHM, are shown.

Changing the thickness of the sample affects the optical thickness, defined as $\tau = d\mu_t$, where d is the thickness of the sample. The measurements made on two different sample thicknesses, 1 and 2 mm, showed a clear difference in the FWHM. In figure 5.7, the resulting FWHM is plotted versus the scattering coefficient.

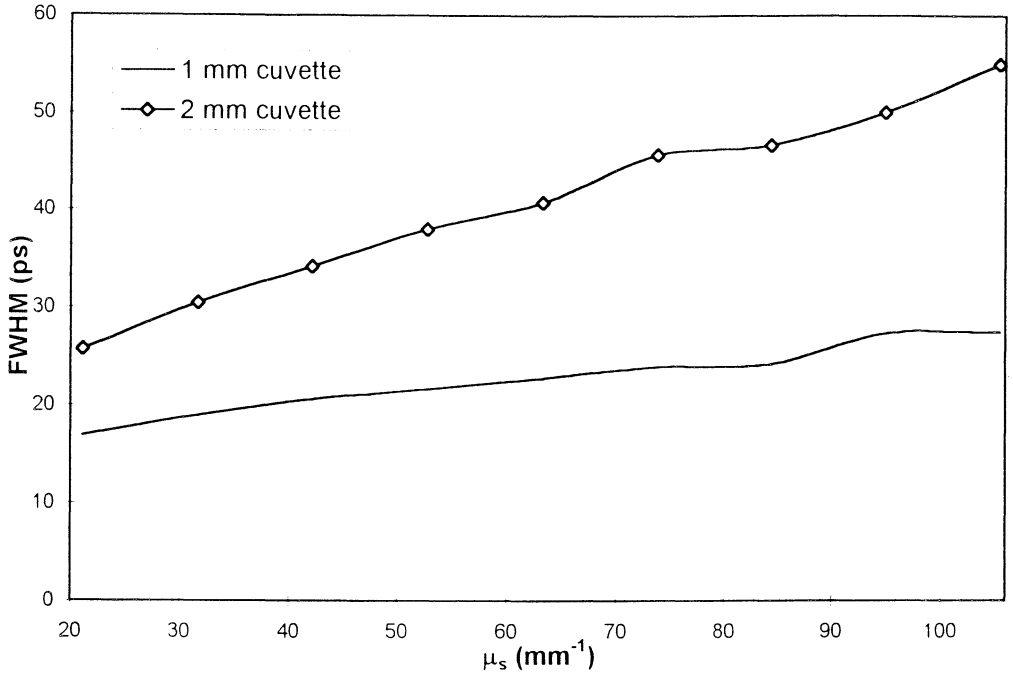

Fig 5.7 The FWHM versus the scattering coefficient for two different sample thicknesses, 1 and 2 mm. Doubling the sample width gives double the increase in FWHM time.

Adding an absorber, in this case ink, to the polystyrene solution changes the attenuation coefficient, μ_t, according to the relation $\mu_t = \mu_s + \mu_a$. The effect is a negative slope for the FWHM with increasing absorption coefficient. The polystyrene sphere concentration was kept at 70% of the total suspension, while increasing the ink concentration in the suspension. The results are shown in figure 5.8. Furthermore, an integrating sphere was placed between the sample and the aperture stop to investigate its effect on the scattering of the detected light. This was performed as the narrow-beam measurement is often performed, by letting the collimated beam first pass through an integrating sphere before it is detected. Results are shown in figure 5.9. At lower scattering coefficients the contribution from the sphere dominates over the contribution from the solution. At approximately μ_s=30 mm^{-1}, the contribution from the sphere is almost 20%.

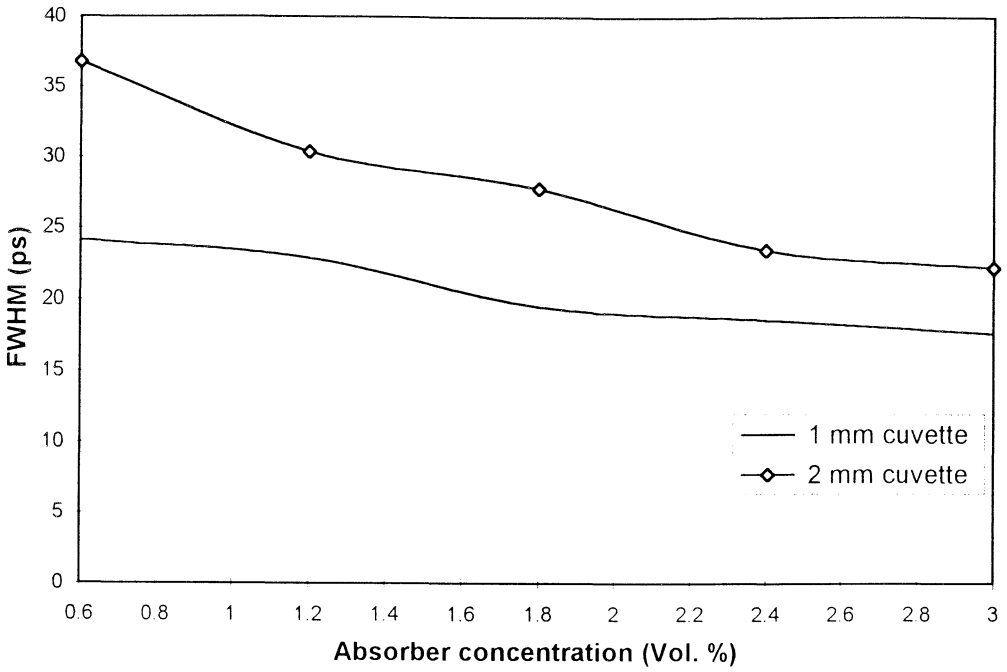

Fig. 5.8 The FWHM versus the absorber concentration in the suspension. The added absorber decreases the timespread in the detected light. Here the polystyrene sphere concentration was kept at 70% of the total susupension, yielding $\mu_s = 73.8\ mm^{-1}$.

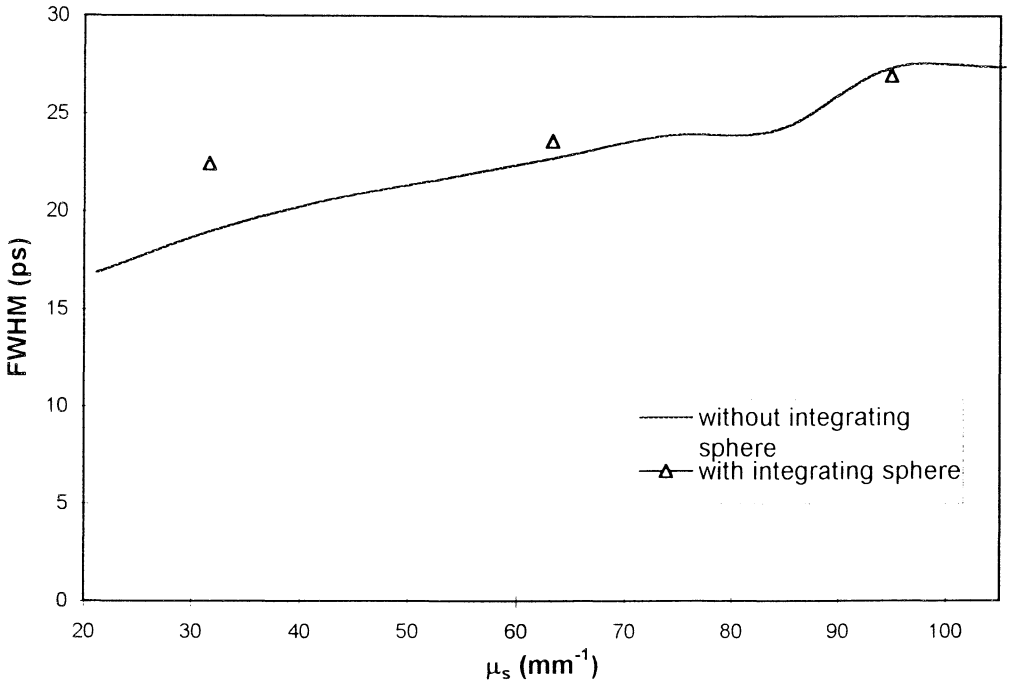

Fig. 5.9 The FWHM versus the scattering coefficient. Placing an integrating sphere in the light beam affects the FWHM at lower scattering coefficients.

A lens was placed between the sample and the aperture stop in order to see whether this increased the amount of detected light or not. The result for a 1.0 mm cuvette is shown in figure 5.10, which shows the FWHM versus the scattering coefficients. More of the scattered light is detected when a lens is put in the beam, after the sample. In the measurements on human blood, there was no increase in the FWHM with increasing blood concentration, as can be seen in figure 5.11. Thus, the scattered light was totally suppressed and not detected.

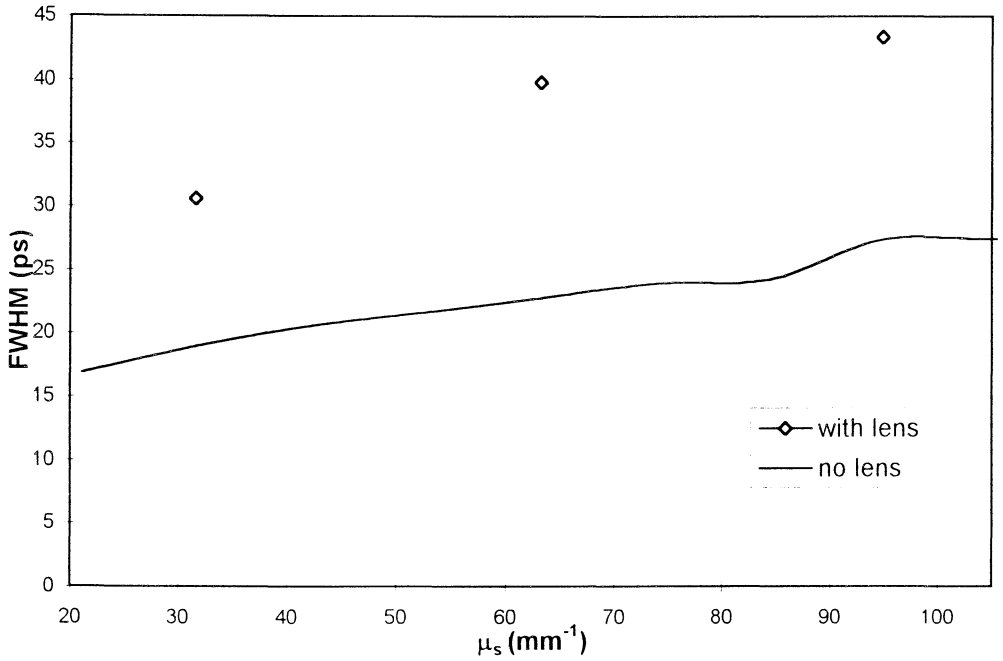

Fig. 5.10 The FWHM plotted against the scattering coefficient for a 1 mm thick sample. As can be seen a lens collects more of the scattered light, giving a broader pulse.

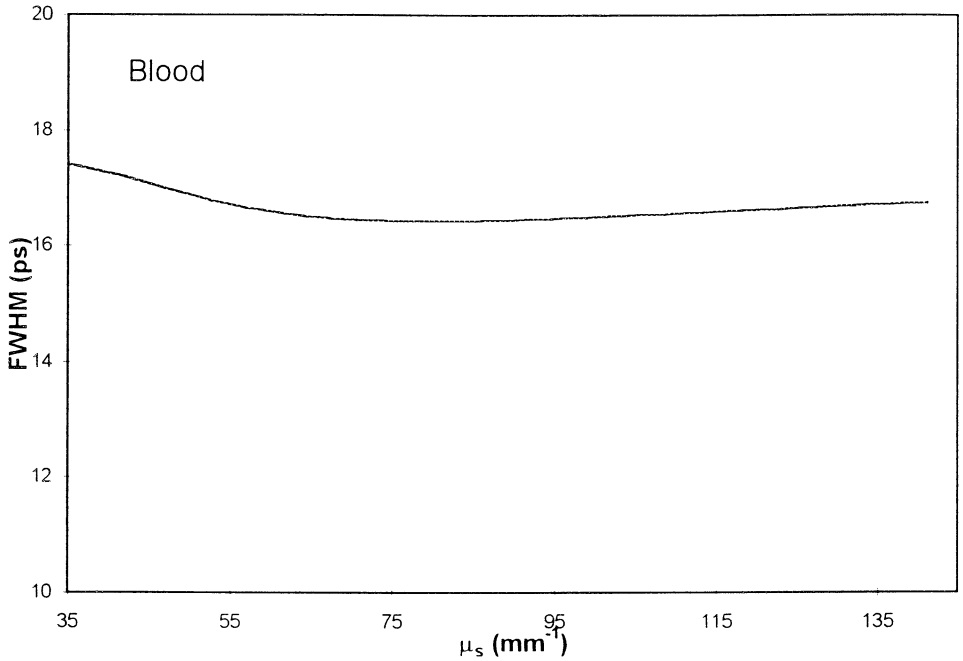

Fig. 5.11 The FWHM for human blood plotted versus the scattering coefficient. The scattered light is totally suppressed.

6 DISCUSSION

The aim of this study was to determine the optical properties of liver tissue that had been treated with thermotherapy and then to compare those results with values for untreated tissue. These changes are important to recognize, as they influence the light distribution in the tissue. They should thus be accounted for in accurate dosimetry of photothermal laser treatment.
Also time-resolved measurements were made to investigate if time resolution can improve the separation of diffusely from collimated transmitted light. This as the narrow-beam measurement often is associated with measurement errors.

6.1 Integrating Sphere Measurements

In this study, the integrating sphere technique was used to determine the optical properties of liver tissue. With this technique it is possible to measure all three optical interaction coefficients. As mentioned above, the most difficult issue is to measure the attenuation coefficient without any effect from scattered light. A highly collimated beam and a small aperture detector was therefore used to reduce any influences of diffusely transmitted light. Similar problems have been discussed in Ref. 7. The remaining two measurements, those of total transmittance and diffuse reflectance, were conducted with an integrating sphere. Approximate values of T_{tot} and R_{diff} are given by Eqs. 4.1 and 4.2. In these simple expressions the assumption has been made that that the total inner surface of the sphere is highly reflective. This is not entirely true since the small sample area has a reduced reflectivity. A more generalized integrating sphere theory which gives more accurate values are discussed in Refs. 33 and 39.
Calibration measurements were made in order to establish the accuracy of the set up, employing these simple expressions. Measurements on the calibration plugs showed a deviation in the order of 2%, see figure 5.1, assuring that the simple Eqs. 4.1 and 4.2 can successfully be applied. To check the narrow-beam measurement, an additional calibration routine was performed with a solution of polystyrene spheres with approximately the same optical properties as those of liver tissue. The agreement between the measured values and those obtained with Mie calculations was very good.
For the experiments, thin *in vitro* samples were used. Of course one should argue that to be able to determine the optical properties of a certain tissue it would be necessary to make *in vivo* measurements. However, with the integrating sphere technique this is not possible. Any changes in the optical properties due to sample preparation must thus be minimized. Since the measurements started immediately after resection the

changes due to sample degradation should be small. Also the main purpose of this work was to investigate the differences between treated and untreated tissue and as all samples were handled in the same way the observed changes could not be due to sample degradation.

A problem with only having one sphere instead of two is that the sample has to be moved in order to be able to perform all three measurements. This makes it important to place the sample accurately relative to the beam so that the same tissue spot is exposed for all three measurements.

Monte Carlo simulations were made to retrieve the optical interaction coefficients from the reflectance and transmittance measurements. This method can be used for every geometry but it requires a lot of computation time. To get a whole set of optical properties it is necessary to perform many inverse Monte Carlo simulations where the measured reflectance and transmittance are fitted to the simulated values. For these calculations a previously developed spline interpolation program and a look-up table with Monte Carlo simulated data were used.[7]

At 800 nm the optical properties for the untreated rat liver tissue were found to be:

$\mu_a = 0.10 \pm 0.02$ mm^{-1}
$\mu_s = 8.3 \pm 0.2$ mm^{-1}
$g = 0.87 \pm 0.02$
$\mu_s' = 1.1 \pm 0.2$ mm^{-1}

The corresponding results for the centrally treated rat liver tissue were:

$\mu_a = 0.31 \pm 0.10$ mm^{-1}
$\mu_s = 10.2 \pm 0.7$ mm^{-1}
$g = 0.67 \pm 0.07$
$\mu_s' = 3.4 \pm 0.9$ mm^{-1}

These results can be compared with data obtained earlier by other authors. For untreated rat liver tissue the corresponding values at 800 nm for Parsa *et al*[40] were:

$\mu_a = 0.67$ mm^{-1}
$\mu_s = 9.2$ mm^{-1}
$g = 0.91$
$\mu_s' = 0.83$ mm^{-1}

showing agreement.

When heating a tissue sample, it has previously been shown[41, 42] that the average size of the scattering centres is changed. In liver the original microscopic scattering structures of the tissue are in the range 500 nm to 1 μm and when heated they coagulate into approximately 100 nm particles.[41] Also these scattering particles are arranged randomly in liver as opposed to for example muscle tissue where there is a repetetive structure. The increase in μ_s for treated tissue is probably a result of the increase in the number of scattering particles, while the decrease in g, *i.e.* the light

was less forward scattered, can be correlated to the decrease in particle size and the random distribution of the scatterers in the tissue. As μ_s was increased and the g-factor decreased, the relation $\mu_s' = \mu_s(1-g)$ predicts an even higher increase in the reduced scattering coefficient as that of the scattering coefficient. Dynamic changes in the optical properties due to heating were not possible to monitor in this *in vitro* study, but may very well be present and have been investigated in connection with heating, for example in Ref. 43. Pickering *et al*[44] have measured the changes in the optical properties of rat liver due to heating. At 1064 nm the increase in the scattering coefficient was 10 % and there was a decrease in both the g-factor and the absorption coefficient, 2.5 % and 5 % respectively. This does not agree with the results obtained in this thesis which at 1050 nm showed an increase in μ_s of on average 25 % and in μ_a an increase of on average 118 %. Furthermore the decrease in g was 11 %. Some probable explanations have been given to this increase in the absorption coefficient. Pickering *et al.*[45] , who have measured the optical properties of slowly heated myocardium, suggest that it is the denaturation of blood that is the reason. This has been verified by Nilsson *et al.*[42] where the increase in the absorption coefficient for heated whole blood is explained by the increased amount of extracellular haemoglobin, which is the main absorber in blood.
The obvious changes in the optical properties when heating a tissue should be recognized and must be considered in laser dosimetry applications.

6.2 Time-resolved measurements

Here investigations were made on a set up measuring the collimated transmittance. Different parameters such as aperture opening and sample thickness were changed in order to determine their effect on the transmittance. Also slight changes was made in the set up by putting a lens and an integrating sphere, respectively, in the light beam. In one of the measurements a 70 %- polystyrene sphere solution diluted with different ink (absorber)-concentrations was used.

Changing the opening of the aperture stop, placed after the sample, did not change the amount of detected light (Fig. 5.6) and for the remaining measurements it was kept at 2.5 cm. The reason for this was probably that the slit of the streak camera efficiently suppressed the scattered light. At lower scattering coefficients, around those for liver tissue, there was a trend showing a difference between the two apertures. When a cuvette with a thickness of 2.0 mm was used, the optical thickness, τ, was doubled as it is directly proportional to d, the thickness of the sample. In figure 5.7 the result with more scattered light detected is shown. When the absorption coefficient was increased, a larger part of the incoming light was absorbed instead of being transmitted, yielding a decrease in the amount of detected light according to figure 5.8. For higher scattering coefficients there was no apparent difference in the detected signal when an integrating sphere, with an open exit port, was placed in the lightbeam as can be seen in figure 5.9. The light pulse was just passing straight through without any interaction. For lower scattering coefficients though, there was a clear

contribution from the sphere in the FWHM-value. This contribution was about 20% when the scattering coefficient was 30 mm^{-1}. As this measurement was performed as the narrow-beam measurements are usually done, this effect has to be taken into account when doing such an experiment. A measurement was also made with the exit port of the sphere blocked and with the light collected by a fibre placed on the side of the sphere, as in the integrating sphere measurements in section 4.1.1. Now the effect of the sphere was obvious. The detected light was now entirely continuous in time. The pulses could not be separated because of the high repetiton rate of the laser, 13 ns, and thus different pulses were integrated in the sphere. Increasing the detection angle by placing a lens behind the sample results in that more of the scattered light is collected. (Fig. 5.10). Highly scattered light that before "missed" the opening on the steak camera is now detected. For the blood measurements, it was clear that, because of the small detection angle used, the collimated transmittance was not influenced by the diffusely transmitted light. This indicates that it is possible to perform accurate narrow-beam measurements, as long as the detection angle is very small.

This set up using the high-power laser system was very sensitive and the effect of reflections from ND-filters and other objects that were not placed exactly perpendicular to the beam caused a lot of trouble. Also the power of the beam varied so that corrections in the number of repressive filters were necessary.

REFERENCES

1. K. Matthewson, P. Coleridege-Smith, J. P. O'Sullivan, T. C. Northfield, and S. G. Bown, "Biological effects of intrahepatic Nd:YAG laser photocoagulation in rats," Gastr. **93**, 550-557 (1987).

2. D. L. Liu, I. Wang, S. Andersson-Engels, C. H Håkansson, U. Stenram, and K. Svanberg, "Intra-operative laser-induced photodynamic therapy in the treatment of experimental hepatic tumours," European Journal of Gastroenterology & Hepatology 7, 1073-1080 (1995).

3. W. F. Cheong, S. A. Prahl, and A. J. Welch, "A review of the optical properties of biological tissues," IEEE J. Quantum Electr. **26**, 2166-2185 (1990).

4. A.Ishimaru, "Diffusion of Light in Turbid Material", Appl. Opt. **28**, 2210-2215 (1989).

5. S. L. Prahl, M. J. C. van Gemert, and A. J. Welch, "Determining the optical properties of turbid media by using the adding-doubling method," Appl. Opt. **32**, 559-568 (1993).

6. M. Keijzer, S. L. Jacques, S. A. Prahl, and A. J. Welch, "Light distribution in artery tissue: Monte Carlo simulations for finite-diameter laser beams," Lasers Surg. Med. **9** 148-154 (1989).

7. A. M. K Nilsson, R. Berg, and S. Andersson-Engels, "Measurements of the optical properties of tissue in conjunction with photodynamic therapy," Appl. Opt. **34**, 4609-4619 (1995).

8. J. C. Hebden, R. A. Kruger, and K. S. Wong, "Time resolved imaging through a highly scattering medium," Appl. Opt. **30**, 788-794 (1991).

9. S. Andersson-Engels, R. Berg, O. Jarlman, and S. Svanberg, "Time-resolved transillumination for medical diagnostics," Opt. Lett. **15**, 1179-1181 (1990).

10. S. Ertefai, and A. E. Profio, "Spectral transmittance and contrast in breast diaphanograhy," Med. Phys. **12**, 393-400 (1985).

11. L.G. Henyey and J.L. Greenstein, "Diffuse radiation in the galaxy," Astrophysical Journal **93**, 70-83 (1993).

12. K.M. Case and P.F. Zweifel, *Linear transport theory*, (Addison-Wesley Publishing Co. 1967).

13. E. Hecht, *Optics*, (Addison-Wesley Publishing Co., 1987).

14. L. Wang, and S. L. Jacques, "Monte Carlo modeling of light transport in multi-layered tissues in standard C," (Laser Biology Research Laboratory, M. D. Andersson Cancer Center, Univ. Of Texas, Houston, Tx., 1992).

15. B. C. Wilson and S. L. Jacques, "Optical reflectance and transmittance of tissue: Principles and applications", IEEE J. Quant. Electr. **26**, 2186-2199 (1990).

16. M. S. Patterson, B. Chance and B. C. Wilson, "Time-resolved reflectance and transmittance for non-invasive measurements of optical properties", Appl. Opt. **28**, 2331-2336 (1989).

17. K. M. Yoo, F. Liu and R. R. Alfano, "When does the diffusion approximation fail to describe photon transport in random media?", Phys. Rev. Lett. **64**, 2647-2650 (1990).

18. F. Liu, K. M. Yoo, and R. R. Alfano, "Ultrafast laser-pulse transmission and imaging through biological tissues." Appl. Opt. **32**, 554-558 (1993).

19. R. Berg, S. Andersson-Engels and S. Svanberg, "Time-resolved transillumination imaging", in *Medical Optical Tomography: Functional Imaging and Monitoring*, G. J. Müller, B. Chance, R. Alfano, S. Arridge, J. Benthan, E. Gratton, M. Kaschke, B. Masters, S. Svanberg, and P. van der Zee, eds., 397-424 (SPIE Optical Engineering Press, Bellingham, Washington, USA, 1993).

20. S. Andersson-Engels, R. Berg, and S. Svanberg, "Effects of optical constants on time-gated transillumination of tissue and tissue-like media," J. Photochem. Photobiol. B: Biol., **16**, 155-167 (1992).

21. S. Andersson-Engels, R. Berg, J. Johansson, K. Svanberg, and S. Svanberg, "Medical applications of laser spectroscopy," in *Laser spectroscopy IX*, M. Feld, J. E. Thomas, and A. Mooradian, eds., 500-504 (Academic Press, Inc, New York, USA, 1989).

22. D. A. Benaron and D. K. Stevenson, "Optical time-of-flight and absorbance imaging of biological media," Science **259**, 1463-1466, (1993).

23. S Andersson-Engels, R. Berg, A. Persson and S. Svanberg, "Multispectral tissue characterization with time-resolved detection of diffusively scattered white light", Opt. Lett. **18**, 1697-1699 (1993).

24. R. Berg, S. Andersson-Engels, C. af Klinteberg and S. Svanberg, "Optical imaging for medical diagnostics using femtosecond white light", in *OSA Proceedings on Advances in Optical Imaging and Photon Migration*, R. R. Alfano, ed., **21** (Optical Society of America, Washington, DC, USA, 1994).

25. J Carlsson, P. Hellentin, L. Malmqvist, A. Persson, W. Persson and C-G Wahlström, " Time-resolved studies of light propagation in paper", Appl. Opt. **34**, 1528-1535 (1995).

26. M. S. Patterson, J. D. Moulton, B. C. Wilson, K. W. Berndt and J. R. Lakowicz, "Frequency-domain reflectance for the determination of the scattering and absorption properties of tissue", Appl. Opt. **30**, 4474-4476 (1991).

27. L. O. Saasand, B. J. Tromberg, R. C. Haskell, T. T. Tsay and M. W. Berns, "Tissue characterization and imaging using photon density waves", Opt. Eng. **32**, 258-266 (1993).

28. S. J. Madsen, E. R. Anderson, R. C. Haskell and B. J. Tromberg, "Portable, high-bandwidth frequncy-domain photon migration instrument for tissue spectroscopy", Opt. Lett. **19**, 1934-1936 (1994).

29. A. E. Profio, "Light transport in tissue," Appl. Opt. **28**, 2216-2222 (1989).

30. L. I. Grossweiner, J. L. Karagiannes, P. W. Johnson, and Z. Zhang, "Gaussian beam spread in biological tissue," Appl. Opt. **29**, 379-383 (1990).

31. R. A. J. Groenhuis, H. A. Ferwerda, and J. J. ten Bosch, "Scattering and absorption of turbid materials determined from reflection measurements. 1: Theory," Appl. Opt. **22**, 2456-2462 (1983).

32. J. W. Pickering, S. A. Prahl, N. Van Wieringen, J. F. Beek, H. J. C. M. Sterenborg, and M. J. C. van Gemert, "Double-integrating-sphere system for measuring the optical properties of tissue," Appl. Opt. **32**, 399-410 (1993).

33. J. W. Pickering, C. J. Moes, H. J. C. M. Sterenborg, S. A. Prahl, and M. J. C. van Gemert, "Two integrating spheres with an intervening scattering sample," J. Opt. Soc. Am. **9**, 621-631 (1992).

34 Christian Sturesson, "Thermodynamical and Biological Aspects of Laser-induced Heat Treatment in Medicine", Lic. thesis, LRAP-203, (Lund Institute of Technology, Sweden, 1996).

35. R. Graaf, J. G. Aarnoudse, J. R. Zijp, P. M. A. Sloot, F. F. M. De Mul, J. Greve, and M. H. Koelink, "Reduced light-scattering properties for mixtures of spherical particles: a simple approximation derived from Mie calculations," Appl. Opt. **31**, 1370-1376 (1992).

36. J. R. Zijp and J. J. ten Bosch, "Pascal program to perform Mie calculations", Opt. Eng. **32**, 1691-1695 (1993).

37. S. Svanberg, J. Larsson, A. Persson, and C.-G. Wahlström, "Lund high-power laser facility - Systems and first results." Physica Scripta **49**, 187-197 (1994).

38. R. R. Alfano, P. P. Ho, and K. M. Yoo, "Photons for prompt tumour detection," Physics World **5**, 37-40 (1992).

39. D. G. Goebel, "Generalized integrating-sphere theory," Appl. Opt. **6**, 125-128 (1967).

40. P Parsa, S. L. Jacques, and N. S. Nishioka, "Optical properties of rat liver between 350 and 2200 nm," Appl. Opt. **28**, 2325-2330 (1989).

41. S. Jaywant, B. Wilson, M. Patterson, L. Lilge, T. Flotte, J. Woolsey, and C. McCulloch, "Temperature dependent changes in the optical absorption and scattering spectra of tissues: correlation with ultra structure," SPIE **1882**, 218-229 (1993).

42. A. M. K. Nilsson, G. W. Lucassen, W. Verkruysse, S. Andersson-Engels, and M. J. C. van Gemert, "Optical properties of human whole blood - changes due to slow heating," SPIE **2923**, 24-34 (1996).

43. S. Rastegar, and M. Motamedi, "A theoretical analysis of dynamic variation of temperature dependent optical properties in the response of laser irradiated tissue," SPIE **1201**, 253-259 (1990).

44. J. W. Pickering, P. Posthumus, and M. J. C. van Gemert, "Continuous measurement of the heat-induced changes in the optical properties (at 1064 nm) of rat liver," Lasers in Surgery and Medicine, **15**, 200-205 (1994).

45. J. W. Pickering, S. Bosman. P. Posthumus. P. Blokland, J. F. Beek, and M. J. C. van Gemert, "Changes in the optical properties (at 632.8 nm) of slowly heated myocardium," Appl. Opt. **32**, 367-371 (1993).